Biochemistry and Biophysics Reports 4 (2015) 312–323

Contents lists available at ScienceDirect

Biochemistry and Biophysics Reports

journal homepage: www.elsevier.com/locate/bbrep

# 1-Amino-4-hydroxy-9,10-anthraquinone – An analogue of anthracycline anticancer drugs, interacts with DNA and induces apoptosis in human MDA-MB-231 breast adinocarcinoma cells: Evaluation of structure–activity relationship using computational, spectroscopic and biochemical studies

Palash Mondal [a,1], Sanjay Roy [b,2], Gayathri Loganathan [c], Bitapi Mandal [d], Dhanasekaran Dharumadurai [c], Mohammad A. Akbarsha [e,f], Partha Sarathi Sengupta [a], Shouvik Chattopadhyay [d], Partha Sarathi Guin [b,*]

[a] Department of Chemistry (UG & PG), Vivekananda Mahavidyalaya, Burdwan 713103, India
[b] Department of Chemistry, Shibpur Dinobundhoo Institution (College), 412/1 G.T. Road (South), Howrah 711102, India
[c] Department of Microbiology, School of Life Sciences, Bharathidasan University, Tiruchirappalli 620024, India
[d] Department of Chemistry (Inorganic Section), Jadavpur University, Raja S.C. Mullick Road, Kolkata 700032, India
[e] Mahathma Gandhi-Doerenkamp Center, Bharathidasan University, Tiruchirappalli 620024, India
[f] Department of Food Science and Nutrition, College of Food Science and Agriculture, King Saud University, Riyadh, Saudi Arabia

ARTICLE INFO

*Article history:*
Received 27 July 2015
Received in revised form
20 October 2015
Accepted 21 October 2015
Available online 23 October 2015

*Keywords:*
1-AHAQ
X-ray diffraction
DFT and spectroscopy
Calf thymus DNA
Apoptosis

ABSTRACT

The X-ray diffraction and spectroscopic properties of 1-amino-4-hydroxy-9,10-anthraquinone (1-AHAQ), a simple analogue of anthracycline chemotherapeutic drugs were studied by adopting experimental and computational methods. The optimized geometrical parameters obtained from computational methods were compared with the results of X-ray diffraction analysis and the two were found to be in reasonably good agreement. X-ray diffraction study, Density Functional Theory (DFT) and natural bond orbital (NBO) analysis indicated two types of hydrogen bonds in the molecule. The IR spectra of 1-AHAQ were studied by Vibrational Energy Distribution Analysis (VEDA) using potential energy distribution (PED) analysis. The electronic spectra were studied by TDDFT computation and compared with the experimental results. Experimental and theoretical results corroborated each other to a fair extent. To understand the biological efficacy of 1-AHAQ, it was allowed to interact with calf thymus DNA and human breast adinocarcinoma cell MDA-MB-231. It was found that the molecule induces apoptosis in this adinocarcinoma cell, with little, if any, cytotoxic effect in HBL-100 normal breast epithelial cell.



## 1. Introduction

Anthracycline drugs are chemotherapeutic agents containing a planar hydroxy-9, 10-anthraquinone at the core of the molecule that is in use for the treatment of various human cancers [1–3]. Although there is controversy regarding the exact mechanism of action of these drugs as chemotherapeutics, various established pathways of drug action such as intercalation into DNA base pairs, inhibition of RNA transcription and DNA replication, inhibition of topoisomerase II, induction of DNA cleavage, etc., were observed to be associated with the interaction of such molecules with DNA [4–10]. A few studies have also shown that the sugar moiety present in these drugs facilitate recognition of cancer cells [9,10]. However, location of the sugar moiety on the aliphatic side chain attached to the hydroxy-9, 10-anthraquinone unit in these molecules makes them so expensive that most patients cannot afford to practice these drugs. This is particularly true of cancer patients belonging to the developing countries. Therefore, efforts are presently afoot to evaluate new but comparatively less expensive substitutes of the known forms of these drugs. Through several studies [11–20], we and others were able to develop less expensive hydroxy-anthraquinone-mimetic drugs. Rossi and coworkers [17] showed that two variant hydroxy-anthraquinones that do not

*Abbreviations:* 1-AHAQ, 1-amino-4-hydroxy-9,10-anthraquinone; DFT, Density Functional Theory; ct DNA, calf thymus DNA; NBO, natural bond orbital; VEDA, Vibrational Energy Distribution Analysis; PED, potential energy distribution

* Corresponding author. Fax: +91 33 2688 0344.
*E-mail address:* parthasg@gmail.com (P.S. Guin).
[1,2] Equal contribution to the article.

http://dx.doi.org/10.1016/j.bbrep.2015.10.008

posses any sugar moiety to exhibit significant chemotherapeutic efficiency. Mitoxantrone, an amino hydroxy -anthraquinone, was found to have better antineoplastic activity and produce lesser toxic side effects than some of the popular anthracycline drugs that are currently in use for treatment of various types of human cancers [18].

In addition to affinity of anthracyclines toward DNA, generation of semiquinone intermediates due to the reduction of the quinone unit by one-electron was found to play a critical role in their chemotherapeutic efficacy [21–23]. However, too much semiquinone formation is harmful [21–23]. The semiquinone reacts with $O_2$ thereby generating superoxide ion ($O_2^{\bullet -}$) and $H_2O_2$/$^{\bullet}OH$ [24,25] that in turn cause various types of harmful effects, rendering a study on redox behavior of such molecules important.

Earlier studies showed that planar anthraquinone unit present in anthracycline drugs intercalates into DNA backbone by π–π stacking and hydrophobic interaction [26,27]. It has been found that intercalation is further stabilized through hydrogen bonding between the bases of DNA and a drug molecule [28,29] which makes the aspects of intra- and intermolecular hydrogen bonding very important for this class of molecules. Deciphering the structure–activity relationship may lead to an introduction of new medicines for a lot of diseases. Such an attempt has been made in the present study so as to lead to a proper understanding of the structure–selectivity relationship of anthracyclines which may lead to bringing up a novel chemotherapeutic agent for the treatment of cancer. Therefore, in the present study we established the structure of 1-AHAQ from single crystal X-ray diffraction. Computational and spectroscopic measurements were performed to understand the electronic state of the molecule and to draw knowledge on hydrogen bonding. In this context it is interesting to note that three-dimensional structures are known only for a few anthracyclines [30,31]. Hence, the three-dimensional structure of 1-AHAQ in the present study might be value-addition to this field of research.

Very recently we reported in detail the electrochemical property of 1-AHAQ [32,33] and its copper complex and showed that the molecule mimics the anthracycline drugs that are already in practice. This was a pointer to us that 1-AHAQ might exhibit a potential antitumor activity as anthracyclines owing to the similarity in electrochemical behavior, an important parameter to determine therapeutic efficiency. Hence, in the present study we subjected 1-AHAQ to analysis cytotoxic potential so as to find its suitability as an anticancer agent. The molecule was allowed to interact with ct DNA and the results correlated with its ability to induce apoptosis in human breast adinocarcinoma cell MDA-MB-231, sparing the normal breast epithelial cells HBL-100.

## 2. Experimental

### 2.1. Materials

1-AHAQ (Scheme 1) (96%), purchased from Alfa Aesar, Germany, was purified and characterized by methods described in our recent reports [32,33]. The pH and ionic strengths of aqueous solutions were maintained by using Hepes buffer and NaCl, respectively (both were of AR Grade, Spectrochem, India). Methanol (HPLC Grade, E-Merck, India), anhydrous acetonitrile (SRL, India), and absolute ethanol (AR Grade) were used in experiments. All other reagents used in the present study were of AR grade. Triple distilled water was used to prepare aqueous solutions. A stock solution of 1-AHAQ in ethanol of strength $10^{-3}$ mol $L^{-1}$ was prepared by accurate weighing of the compound as it is almost insoluble in water. For the experiments in aqueous media, the stock ethanol solution of the compound was diluted quantitatively with water.

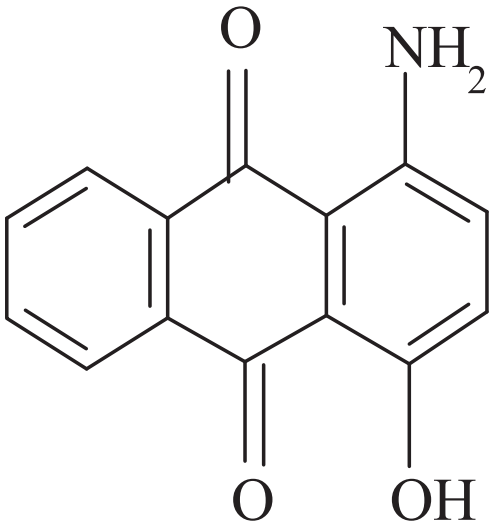


**Scheme 1.** 1-Amino-4-hydroxy-9,10-anthraquinone.

All solutions of the compound were made just before the experiment and stored in the dark as it is photosensitive. Calf thymus DNA (ct DNA) (SRL, India) was dissolved in aqueous buffer and the purity of it was checked from the ratio of the absorbance of the solution at 260 and 280 nm ($A_{260}/A_{280}$). The experimental solutions showed that the ratio was in the range $1.8 < A_{260}/A_{280} < 1.9$ which provided a good estimate of the purity of the DNA [34]. The concentration of experimental DNA solution was evaluated in terms of nucleotide by considering $\varepsilon_{260}=6600\ M^{-1}\ cm^{-1}$ for ct DNA. Single-stranded DNA was prepared by using the method as described by Silva et al. [35].

### 2.2. Crystallographic analysis

A suitable single crystal of 1-AHAQ was subjected to diffraction with graphite-monochromated Mo-Kα radiation ($\lambda=0.71073$ Å). The evaluated experimental data was integrated by SAINT [36] and absorption corrections were done using SADABS. Structure was resolved using SHELXS 97 adopting Patterson method [37] which was then followed by consecutive Fourier and difference Fourier synthesis. In the present study full-matrix least-squares refinement was done on F2 by via SHELXL 97 [37] with the anisotropic displacement parameters for all the non-hydrogen atoms [38]. During refinement, data were subjected to calculations adopting SHELXL 97, SHELXS 97, PLATON v1.15, ORTEP-3v2 and WinGX v1.80 [39–41]. Some important parameters of crystallographic analysis and structure and bonding are summarized in Tables 1 and S1 (Supporting information), respectively.

### 2.3. Computational methods

Hartree-Fock (HF) and Density Functional Theory (DFT), for example B3LYP and PBEPBE [42–44], were applied to determine the fully unconstrained geometry optimization and energy calculation on the molecule. To incorporate the effect of the solvent, conductors like polarized continuum medium (CPCM) [45–48] were employed.

Vibrational Energy Distribution Analysis (VEDA) 4.0 [49] was used to calculate potential energy distribution (PED). The modes of vibration of the molecule were assigned precisely by using PED values and visual check up with Gauss View 4.1. Natural bond orbital analysis (NBO) at B3LYP/6-31+G (d, p) was applied to recognize orbital interactions, natural atomic charges and

delocalization of charge in the equilibrium geometry of 1-AHAQ with the help of NBO 3.1 [50–52]. In this study, NBOs were first defined for each covalent bond, lone pair, and anti-bonding orbital by using the molecular orbitals obtained by quantum chemical calculations [53] estimated by using second order perturbation theory. The expression of stabilization energy E(2) associated with NBO Fock matrix element for each donor and acceptor NBO (i and j, respectively) can be shown as

$$E(2)=\Delta E_{ij} = q_i \frac{F(i,j)^2}{\varepsilon_j - \varepsilon_i} \quad (1)$$

where $q_i$=donor orbital occupancy, $\varepsilon_i$ and $\varepsilon_j$=diagonal elements and $F(i,j)$=off diagonal NBO Fock matrix element. The quantum chemical computations were done with Gaussian 09 package [54].

### 2.4. Spectroscopic and electrochemical studies

FTIR in the range of 500–4000 $cm^{-1}$ was measured in Perkin Elmer RX-I spectrophotometer by using KBr pellets. UV–vis studies were done using the spectrophotometer, Model: MECASYS OPTIZEN POP, South Korea. Electrochemical measurements were carried out by using a three- electrode system and the potentiostat, Digi-Ivy, Model DY2312. In this case the working electrode was a glassy carbon electrode having surface area 0.07065 $cm^2$, the reference electrode was Ag/AgCl, saturated KCl whereas the counter electrode was a platinum wire. During these experiments temperature was maintained at 298.15 K with the help of a circulating water bath. To avoid the effect of dissolved oxygen in the electrochemical studies all solutions were degassed before the experiment for 45 min by using high-purity argon.

### 2.5. Cell culture

The MDA-MB-231 human breast adinocarcinoma cells and HBL-100 normal breast epithelial cells were provided by National Center for Cell Science (NCCS), Pune, India. DMEM medium (Sigma–Aldrich, St. Louis, MO, USA), supplementd with 10% fetal bovine serum (Gibco), was used to culture the cells. Penicillin (100 U/mL) and of streptomycin (100 µg/mL) (Gibco) were used as antibiotics. The cells were cultured in 96 well plates in a $CO_2$ incubator (Thermo Scientific, USA). The culture conditions included 37 °C, humidified atmosphere and 5% $CO_2$. Care was taken to use cells belonging to passage 15 or less.

### 2.6. Cytotoxicity assay (MTT assay)

For the cytotoxicity assay 1-AHAQ was dissolved in DMSO. The concentration was in the range 20–200 µM. The MDA-MB-231 cells were seeded at $5 \times 10^3$ cells per well in 200 µL of fresh culture medium. The test substance was added to the wells 24 h after seeding DMSO solution was treated as solvent control. The cell viability/growth inhibition was assessed using the MTT [3-(4,5-dimethylthiazol-2-yl)-2,5-diphenyl-2H-tetrazolium bromide] method, according to Mosmann [55]. The MTT solution, 5 mg/mL, was prepared in phosphate-buffered saline (PBS). After incubation for 24 h and 48 h, 20 µL of MTT solution was added to each well. The plates were incubated for 4 h at 37 °C in dark. The reaction resulted in formation of purple formazan, which was dissolved in of 100 µL of DMSO added to each well. The OD was read in a 96-well plate reader (Bio-Rad, Hercules, CA, USA) at 570 nm (measurement) and 630 nm (reference). The experiments were conducted in triplicates. and the data were used for calculating the mean percentage inhibition. The following formula was used:

$$\text{Percentage inhibition} = \frac{[\text{Mean OD of untreated cells(control)} - \text{Mean OD of treated cells(treated)}] \times 100}{\text{Mean absorbance of untreated cells(control)}}$$

A standard curve was prepared by plotting % inhibition against concentration, and the concentration of the test substance which reduced the viability to 50% ($IC_{50}$) was deduced.

### 2.7. Acridine orange (AO) and ethidium bromide (EB) staining

The morphological changes in cells that would reveal if cell death occurs via apoptosis or necrosis were analyzed adopting acridine orange (AO) and ethidium bromide (EB) staining [56]. MDA-MB-231 cells were seeded into the wells of 6 well plate at an initial density of $5 \times 10^5$ cells per well. After attachment the cells were exposed to 1-AHAQ at its 24 h $IC_{50}$ concentration. After incubation the cells were stained with AO - EB solution (AO – 3.8 µM; EB – 2.5 µM of EB in PBS; 25 µL to each well) and examined in a fluorescent microscope (Carl Zeiss, Jena, Germany) at 450–490 nm. Three hundred cells per well were counted in triplicate. The cells were scored as viable, apoptotic or necrotic as judged by based on the morphological changes as revealed in the color, morphology of nuclei and integrity of the membrane [56] the cells were assigned as viable, apoptotic or necrotic. From this data percentages of cells in apoptosis and necrosis were calculated. Cells reflecting morphological changes of interest were photographed.

### 2.8. Hoechst 33528 Staining

For assessment of nuclear morphological changes MDA-MB-231 cells were cultured in 6-well plates and treated with the 24 h $IC_{50}$ concentration of 1-AHAQ. The cells were stained for 5 min with an aqueous solution of Hoechst 33258 (1 mg/mL) [57]. A drop of cell suspension was loaded onto a glass slide and covered with a coverslip. At random 300 cells were observed at 400× in a fluorescent microscope (Carl Zeiss, Jena, Germany). The cells were counted in three fields each, and classified as normal or pathological, and the data were converted to the respective percentages.

**Table 1**
Crystallographic data and refinement details for 1-amino-4-hydroxy-9,10-anthraquinone.

| Formula | $C_{14}$ $H_9$ N $O_3$ |
|---|---|
| Formula weight | 239.22 |
| Crystal system | Triclinic |
| Space group | P1 |
| $a$ (Å) | 3.8012(1) |
| $b$ (Å) | 9.6978(3) |
| $c$ (Å) | 14.3666(5) |
| $\alpha$ (deg) | 90 |
| $\beta$ (deg) | 96.671(2) |
| $\gamma$ (deg) | 90 |
| $V$ (Å$^3$) | 526.01(3) |
| $Z$ | 2 |
| $D_{calc}$ (g/cm$^3$) | 1.510 |
| $\mu$ (mm$^{-1}$) | (MoKα) 0.108 |
| Temperature (K) | 293 |
| Total Uniq. Data $R$(int) | 6281, 2789, 0.018 |
| Observed data I $> 2\sigma$(I) | 2524 |
| R, wR2, S | 0.0300, 0.0818, 1.05 |
| Min. and Max. Resd. Dens. [e/ Å$^3$] | −0.15, 0.12 |

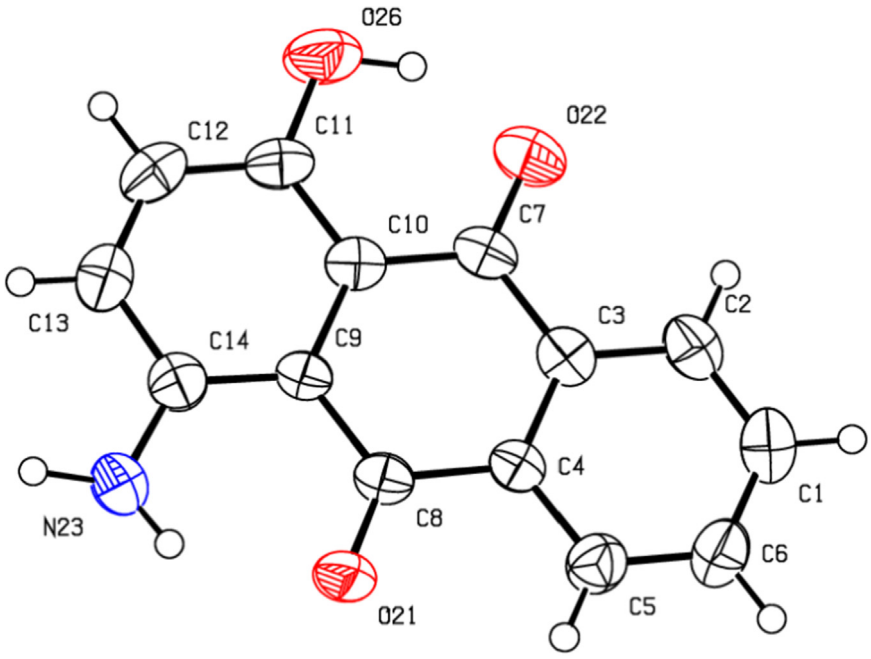


**Fig. 1.** X-ray crystallographic structure of 1-AHAQ (per unit cell two identical molecules are present).

**Table 2**
Hydrogen bond lengths [Å] and angles [deg] for 1-amino-4-hydroxy-9,10-anthraquinone.

| D-H…A | D-H | H….A | D….A | ∠D-H….A |
|---|---|---|---|---|
| N23-H24……O21 | 0.90(3) | 1.96(3) | 2.662(3) | 134(2) |
| N23-H25…….O21 | 1.00(4) | 2.11(4) | 3.078(3) | 163(3) |
| O26-H27…….O22 | 0.99(3) | 1.62(4) | 2.507(3) | 146(3) |

D is donor and A is acceptor.

## 3. Results and discussion

### 3.1. Structure of 1-AHAQ from crystallographic methods

Analysis of single crystal structure of 1-AHAQ showed that it crystallizes in the triclinic space group P1 (Table 1) in which two identical molecules are present per unit cell (only one molecule is shown in Fig. 1 as the two are identical). The bonding parameters are shown in Table S1 (Supporting information) from which it is clear that C7–O22, C8–O21, C11–O26, C14–N23 and N23–H24 bond lengths are considerably shorter than typical single C–O (1.38–1.42 Å), C–N (1.44-1.47 Å) and N–H (1.00) bonds while the O26–H27 bond length (0.99 Å) is longer than typical single O–H (0.94–0.96) bonds. The two hydrogen bonds are shown in Fig. 1 (Table 2). These two hydrogen bonds of 1-AHAQ are connected by N23–H24….O21 (2.662 Å, 134°) and O26–H27…O22 (2.507 Å, 146°) (Table 2) which is comparable to that observed in an earlier study by Zhu et al. [58].

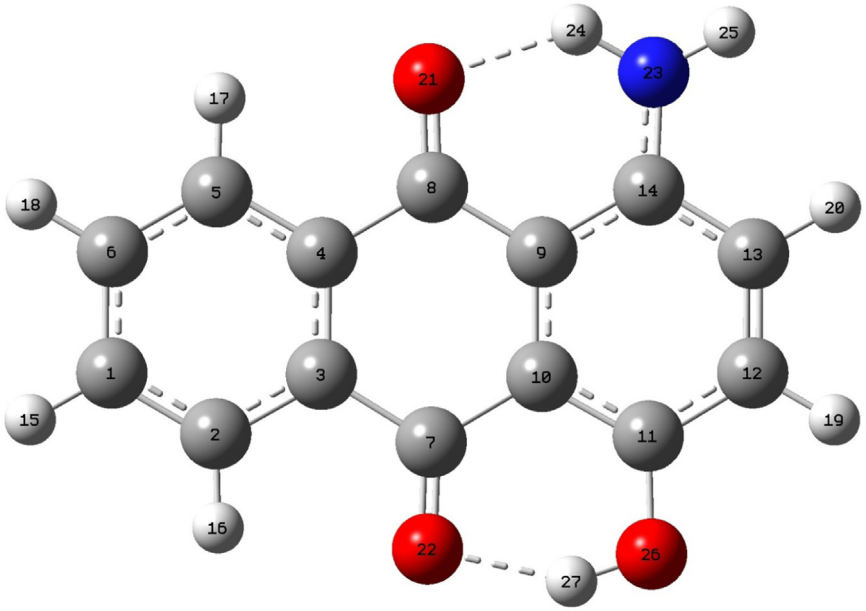


**Fig. 2.** Optimized molecular structure of 1-amino-4-hydroxy-9,10-anthraquinone using B3LYP/6-31+G(d,p) protocol.

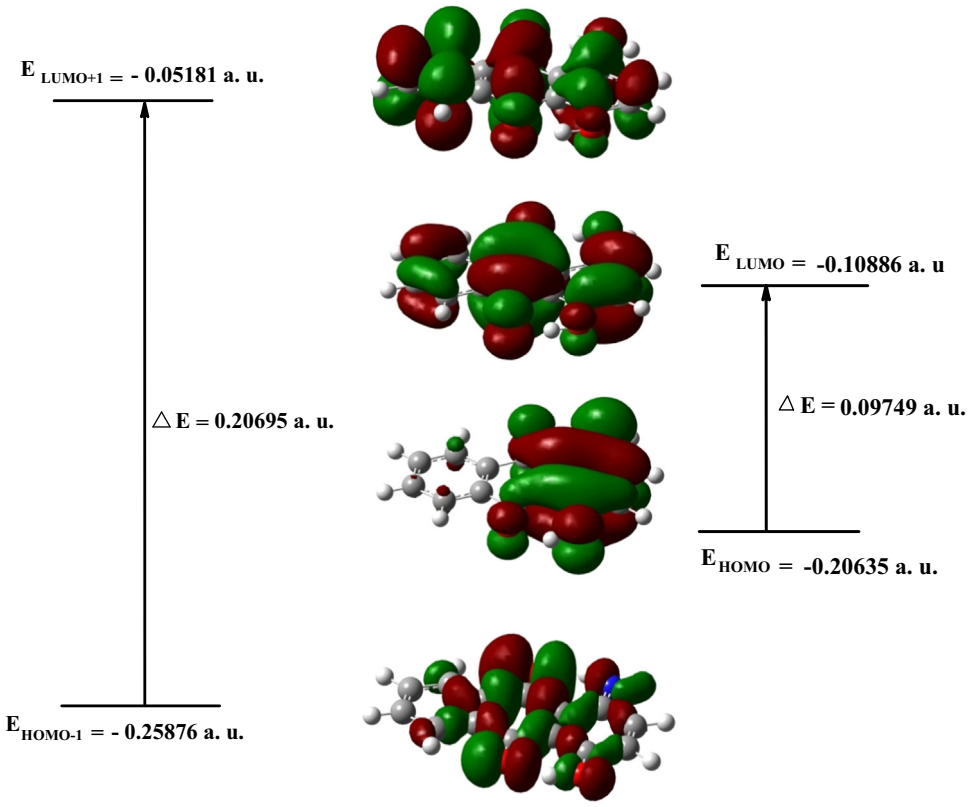


**Fig. 3.** The isodensity plot of HOMO, LUMO, HOMO-1 and LUMO+1 for 1-amino-4-hydroxy-9,10-anthraquinone.

### 3.2. Structure of 1-AHAQ deduced from computational methods

Optimized structure of 1-AHAQ is shown in Fig. 2 for which the minimum energy values were observed as −814.515, −819.423 and −818.477 a.u. for HF, B3LYP and PBEPBE, respectively. The difference in the values of energy was observed to be dependent on the methods of calculation. Thus, the absolute value of electronic energy depends on the methods of calculation. The most important bonding parameters are shown in Table S1 (Supporting information). As found in the single crystal structure of the molecule, hydrogen bonding between O21 and H24 and O22 and O27 were established in this case which is discussed in NBO analysis (Section 3.5.). Comparison of the experimental with theoretical bonding parameters showed a very slight deviation between the two which is probably due to the fact that computational studies were carried out on an isolated gaseous molecule whereas the experimental results were evaluated in the solid state.

The frontier molecular orbital (FMO) of a molecule consists of highest occupied molecular orbital (HOMO) and lowest unoccupied molecular orbital (LUMO). A consideration of such orbitals is very much helpful in determining the way in which a molecule such as 1-AHAQ molecule interacts with a biological macromolecule such as DNA [59]. The chemical reactivity of a molecule in terms of electronic behavior is related to the energy gap in FMO since HOMO acts as an electron donor while LUMO acts as an electron acceptor. The energy gap between HOMO and LUMO in the present study was determined as 0.097 a.u. The isodensity plot of FMOs are shown in Fig. 3 from which it is clear that HOMO looks as delocalized p-type and LUMO as localized p-type.

### 3.3. Theoretical and experimental IR spectra of 1-AHAQ

VEDA [50] with PED analysis was employed to analyze theoretical vibrational spectrum of 1-AHAQ [33]. In this method, some normal modes are extended over the entire molecule and PED is accounted for certain levels [33]. This enables one to describe the contribution to the movement of a given group of atoms in a normal mode quantitatively [33]. Data from theoretical IR spectral analysis was compared with experimental results to see whether 1-AHAQ is in the ground state or in any transition state. For transition state of a molecule at least one imaginary frequency should be present in the theoretical studies. However, in the present calculation all the theoretical IR bands are positive which means that 1-AHAQ is in the ground state. This further supports the structure of 1-AHAQ obtained both from the crystallographic and density functional methods. 1-AHAQ contains 27 atoms and its optimized molecular structure exhibits 75 fundamental vibrations which are IR active, out of which 26 are stretching, 25 are bending and 24 are torsion. The computed vibrational frequencies are overestimated and scaled 0.9613 for B3LYP/6-31+ G (d, p) level of computation [49]. IR frequency and intensity, PED and description about the modes of vibration for 1-AHAQ are shown in Table S2 (Supporting information). Comparing the theoretical and experimental bands (Table S2 and Fig. S1) (Supporting Information) it may be concluded that both the results corroborate excellently in the region below 3000 $cm^{-1}$. However, a deviation appears between theoretical and experimental IR intensities in the region 3000 $cm^{-1}$ and above which may be due to the hampering of crystal field spectra [60].

### 3.4. UV–vis spectroscopy of 1-AHAQ

In 30% ethanol the absorption spectra of 1-AHAQ show four peaks at 248, 288, 530 and 565 nm [Fig. S2 (Supporting information)]. In aqueous media 1-AHAQ exists in different tautomeric forms due to keto-enol tautomerism which remain in very rapid equilibrium [61]. The $\pi$–$\pi^*$ and n–$\pi^*$ transitions of such tautomeric structures result in the above-mentioned absorption peaks [33].

**Table 3**
The experimental and theoretical $\lambda_{max}$ of bands of 1-amino-4-hydroxy-9, 10- anthraquinone along with the molecular orbitals involved in the transitions.

| Experimental band ($\varepsilon$, $dm^3\ mol^{-1}\ cm^{-1}$) | TD-DFT peaks (oscillator strength) | Contribution |
|---|---|---|
| 565 | 499 (0.1633) | HOMO→LUMO |
| 530 | 402 (0.0006) | (HOMO-1)→LUMO |
| 288 | 287 (0.055) | HOMO→(LUMO+2) |
| 288 | 278 (0.1205) | (HOMO-3)→(LUMO+2) |
| | | (HOMO)→(LUMO+3) |
| | | (HOMO)→(LUMO+5) |
| | | (HOMO-5)→(LUMO) |
| | | (HOMO-6)→(LUMO) |
| 248 | 235 (0.3275) | (HOMO-3)→(LUMO+1) |
| | | (HOMO-3)→(LUMO+2) |
| | | (HOMO-2)→(LUMO+1) |
| | | (HOMO-2)→(LUMO+2) |
| | | (HOMO) →(LUMO+3) |

TDDFT method was applied to characterize the nature of orbitals involved in such transitions and to justify the experimental findings with theoretical values. The theoretical and experimental absorption spectra of 1-AHAQ are shown in Fig. S2 (Supporting information) and the absorption maxima $\lambda_{max}$ and nature of different atomic orbitals in the molecular orbitals associated with the transitions are shown in Tables 3 and S3 (Supporting information), respectively. Theoretical results established that several atomic orbitals combine to produce a molecular orbital. By applying DFT procedure, the molecular orbitals involved in transitions were determined and are shown in Fig. 4. From Fig. 4 it is clear that HOMO is due to π-orbitals present in the ring while LUMO is of $\pi^*$ character. The study suggests that theoretical absorption spectra corroborate the experimental result of the molecule very nicely.

### 3.5. NBO analysis

Intermolecular recognition is a key process for the interaction of a molecule with biological systems. The strength of intra- and intermolecular weak interactions including aromatic stacking, binding and intercalation, Van der Waals interactions, hydrogen bond formation, etc., are closely related to the biological activity of a molecule [59]. Such interactions can be explained by NBO analysis as it provides knowledge about the interactions in both filled and virtual orbitals of a molecule. The values for the second order perturbation energy ($E^{(2)}$) associated with NBO Fock matrix element are mentioned in Table S4 (Supporting information). The large values of $E^{(2)}$ (158.71, 108.00, 93.24 and 80.46 kcal/mol) [Table S5 (Supporting information)] are indicative of very strong hyperconjugative interactions in the aromatic ring system of 1-AHAQ. The hyperconjugative interaction and electron density delocalization of lone pairs from $O_{22}$ to the antibonding orbital of $O_{26}$–$H_{27}$ in the $O_{26}$–$H_{27}$…..$O_{22}$ moiety [LP(1) $O_{22}$→BD*(1) $O_{26}$–$H_{27}$, LP (2) $O_{22}$→BD*(1) $O_{26}$–$H_{27}$] were evaluated in the present study [Table S4 (Supporting information)]. In the same way, lone pairs of $O_{21}$ were observed to be delocalized to the antibonding $N_{23}$–$H_{24}$ $\sigma^*$ orbital [LP(1) $O_{21}$→BD*( 1) $N_{23}$–$H_{24}$ and LP(2) $O_{21}$→BD*( 1) $N_{23}$–$H_{24}$] in $N_{23}$–$H_{24}$…$O_{21}$ moiety. The intramolecular charge transfer in both cases clearly indicates the presence of the intramolecular hydrogen bond (IHB). The geometrical parameters found in the optimization process [Table S1 (Supporting information)] also favor the presence of hydrogen bonds in $O_{22}$…$H_{27}$–$O_{26}$ and $O_{21}$….$H_{24}$–$N_{23}$ moiety.

In order to derive knowledge about hydrogen bonding between ($O_{22}$ ...$H_{27}$–$O_{26}$) and ($O_{21}$ ...$H_{24}$–$N_{23}$), population analysis was done in MO62X DFT protocol with 6-311+ g (d,p) basic set in conductor such as polarized continuum medium (CPCM). Global- hybrid meta GGA MO62X DFT protocol implemented by Truhlar group [62,63] was fitted to evaluate medium range dispersion interactions. Wiberg bond indices [64] are a measure of the bond interaction between two atoms and function as a nominal bond order which were determined by using NBO analysis. In the present case it established an overlap involving a hydrogen atom in $O_{22}$…$H_{27}$–$O_{26}$ and $O_{21}$….$H_{24}$–$N_{23}$ moieties, which means that the hydrogen bonds are not purely electrostatic in character. Wiberg bond indices for the two hydrogen bonds were observed as 0.0926 and 0.0215 for $O_{22}$...$H_{27}$ and $H_{24}$….$O_{21}$, respectively, which clearly shows that $O_{22}$...$H_{27}$ is a strong hydrogen bond while $H_{24}$….$O_{21}$ is a weak hydrogen bond. The information about the strength of hydrogen bonds obtained from the Wiberg bond indices justifies the information on hydrogen bonds obtained from the crystallographic and energy-optimized results of the present molecule.

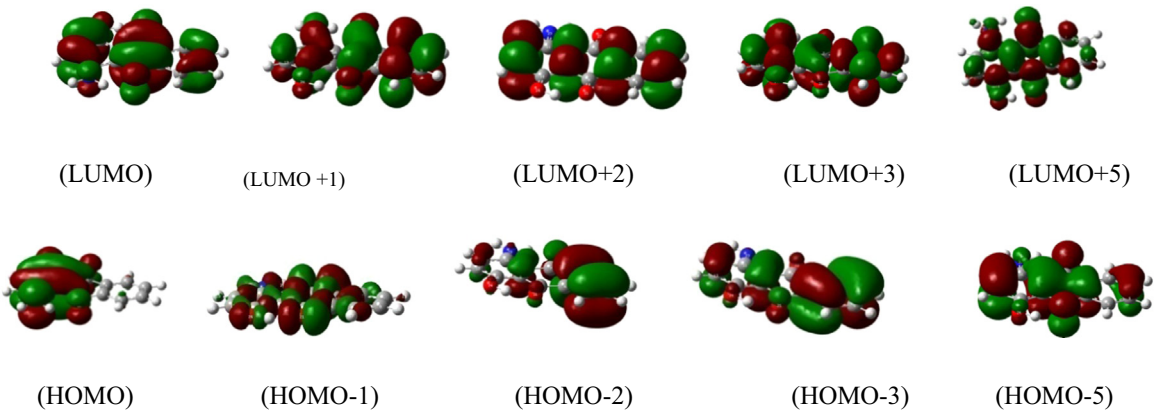


**Fig. 4.** Important molecular orbitals involved in electronic transitions of 1-amino-4-hydroxy-9,10-anthraquinone.

### 3.6. Electrochemical reduction of 1-AHAQ in aqueous media

In our very recent studies [32,33] we observed that 1-AHAQ undergoes single step quasi-reversible reduction by two electrons in aqueous media at neutral pH (7.0). The electrochemical aspect of the molecule at physiological pH (7.4) is an important step for a molecule in determining its biological action. However, in earlier studies [32,33] the electrochemical reduction of 1-AHAQ was not studied in aqueous buffer at physiological pH (7.4) and that is the reason why in the present study we report the redox behavior of 1-AHAQ in aqueous solution at pH 7.4. This shows a quasir-eversible two-electron reduction at –665 mV corresponding to the reduction of quinone to quinone dianion [Fig. S3 (Supporting information)]. The formal reduction potential was observed as −650 mV. Chronocoulometric measurements were done to determine the number of electrons concerned in this reduction. The quinone dianion generated in this process is stabilized by solvent water molecules through hydrogen bonds thereby making the process irreversible [32]. However, with the increase in scan rate the reduction becomes increasingly reversible which might be due to the fact that at higher scan rate quinone dianion gets smaller time to be stabilized by solvent water molecules. In aqueous media, anthracycline drugs adriamycin, daunorubicin, idarubicin, etc., [65–68] also undergo two-electron reduction, as observed in case of 1-AHAQ, that leads to a similarity in electrochemical behavior in such media. We observed that the electrochemical property of the present molecule is governed by several factors such as solvent polarity, existence of acidic or basic species in the media, character of supporting electrolyte, intra- and intermolecular hydrogen bonding, homogeneous chemical reaction, etc., in both aqueous and non-aqueous media [32]. This property of 1-AHAQ exactly mimics the established anthracycline drugs in every step of the electrochemical actions [32] which raises the expectation that it might exhibit a potential antitumor activity.

### 3.7. Investigation on the interaction of 1-AHAQ with calf thymus DNA

In aqueous media containing 2% ethanol at physiological pH (7.4), in the presence of 120 mM NaCl, the absorption spectrum of 1-AHAQ was as shown in Fig. 5a which exhibits an absorption peak at 530 nm. To study the 1-AHAQ–DNA interaction, a set of experimental solutions was prepared consisting of a fixed concentration of 1-AHAQ ([1-AHAQ]=20 μM) and variable concentrations of ct DNA. The absorbance of such solutions were measured at 530 nm and applied to determine the binding parameters. The change in absorption spectra of the compound with increasing amount of DNA is shown in Fig. 5a which clearly indicates a hypochromic effect along with a slight bathochromic shift with the increase in concentration of DNA. These shifts were produced as the result of the electronic interaction owing to the intercalation of the compound chromophore into DNA backbone [68–71]. In order to check whether hypocromism in the absorption spectra of 1-AHAQ upon addition of DNA might be related to a precipitation of 1-AHAQ rather than to its interaction with DNA, different sets of solutions containing a constant concentration of 1-AHAQ (20 μM) and different concentrations of ethanol [Fig. S4 (Supporting information)] were prepared and UV–vis spectra were measured. From this figure it is clear that in the presence of different concentrations ethanol, the UV–vis spectra and hence the absorbances of 1-AHAQ at 530 nm do not alter significantly. Thus it may be said that hypocromism in the UV–vis spectra of 1-AHAQ in DNA interaction study was due to the interaction of 1-AHAQ with DNA but not due to a precipitation of the molecule in the reaction media. In our very recent study [72], by using cyclic voltammetry as monitoring technique we also established that 1-AHAQ interacts with DNA which results in a decrease in the reduction peak current of 1-AHAQ under the similar experimental condition as we used in the present study. In that study [72] we also observed no precipitation of 1-AHAQ in the reaction media since a precipitation of an experimental molecule (1-AHAQ) can cause a great disturbance in the electrochemical setup and it was not possible to carry out a DNA interaction using cyclic voltammetry.

Depending on the change in absorbance of 1-AHAQ at 530 nm upon its interaction with DNA, the apparent binding constant ($K$) was evaluated by using Eq. (2) [73].

$$\frac{A^0}{A-A^0} = \frac{\varepsilon}{\varepsilon_b-\varepsilon} + \frac{\varepsilon}{\varepsilon_b-\varepsilon}\frac{1}{K[DNA]} \quad (2)$$

where $A^0$ and $A$ = absorbances of 1-AHAQ in the absence and in the presence of DNA at 530 nm; $\varepsilon$ and $\varepsilon_b$ = molar extinction coefficients of 1-AHAQ and DNA.1-AHAQ, respectively.

A plot of $A_0/(A-A_0)$ vs. the inverse of the concentration of DNA according to Eq. (2) (Fig. 5b) is a straight line which produced K as $(1.09 \pm 0.11) \times 10^4\ M^{-1}$.

The outcome of the spectrometric studies on 1-AHAQ–DNA interaction was also analyzed using non-linear method assuming the equilibrium as described in Eq. (3) [12,14–16,74–78].

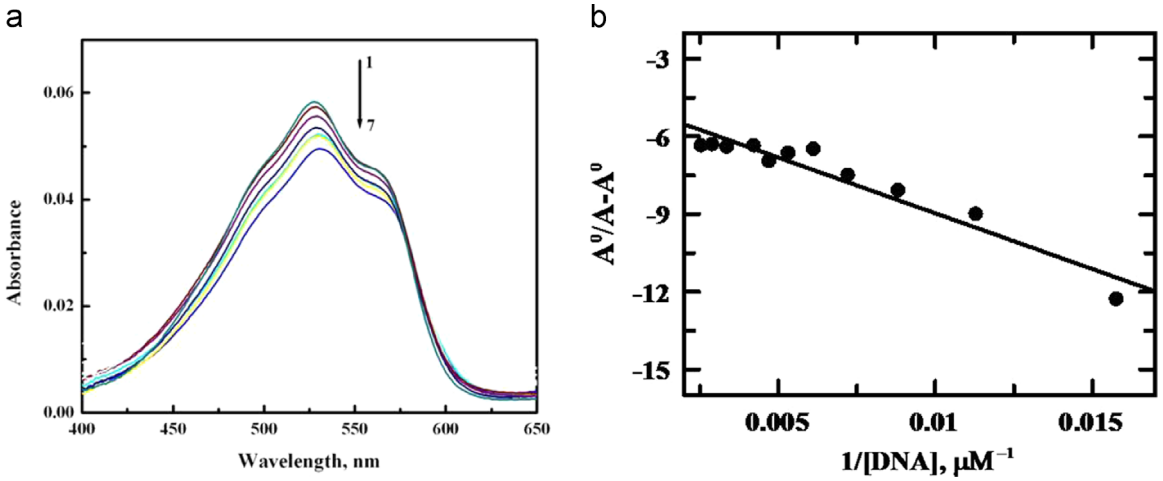


**Fig. 5.** (a). Absorption spectra of 1-AHAQ (20 μM) in the absence (Curve-1) and in the presence of different calf thymus DNA concentrations (Curve- 2–7). pH=7.4, [NaCl]= 120 mM, 25 °C. (b). Double reciprocal plot, ($A_0/A-A_0$) vs. 1/[DNA], of 1-AHAQ–calf thymus DNA interaction; $[1\text{-AHAQ}]_0$ = 20 μM, pH=7.4, [NaCl]=120 mM, 25 °C.

$$1-AHAQ + DNA \rightleftharpoons DNA.1-AHAQ \quad (3)$$

The equilibrium constant for the dissociation of DNA.1-AHAQ species may be represented as:

$$K_d = \frac{[1-\mathrm{AHAQ}][\mathrm{DNA}]}{[\mathrm{DNA.\ 1-AHAQ}]} \quad (4)$$

$$K_d = \frac{\{[1-\mathrm{AHAQ}]_0 - [\mathrm{DNA.\ 1-AHAQ}]\}\{[\mathrm{DNA}_0]-[\mathrm{DNA.\ 1-AHAQ}]\}}{[\mathrm{DNA.\ 1-AHAQ}]} \quad (5)$$

where, $[1\text{-AHAQ}]_0$=concentration of 1-AHAQ which was constant in all the titration mixtures and $[\mathrm{DNA}_0]$=concentration of DNA in the solution. The apparent binding constant may then be determined by taking the inverse of the dissociation constant (i.e., $K=1/K_d$). In the present study, the concentration of 1-AHAQ was 20 μM while that of DNA was reserved 20–25-fold higher than the compound. Basic assumption of the present study is that the DNA concentration must be much greater than the concentration of the compound (1-AHAQ). Now, if $C_0=[1\text{-AHAQ}]_0=20$ μM while $C_D=[\mathrm{DNA}_0]$=DNA concentration in the solution, then

$$K_d = \frac{\{C_0-[\mathrm{DNA.\ 1-AHAQ}]\}\{C_D-[\mathrm{DNA.\ 1-AHAQ}]\}}{[\mathrm{DNA.\ 1-AHAQ}]} \quad (6)$$

The change in absorbance of 1-AHAQ owing to the addition of DNA can be given as $\Delta A=(A^0-A)$. $\Delta A_m$ is the same parameter when 1-AHAQ is totally combined to DNA. During the entire experiment, both free 1-AHAQ and its bound form with DNA (i.e., 1-AHAQ.DNA) contribute to the observed absorbance. Thus, $\Delta A$ may be expressed as $(\varepsilon c_f^i - \varepsilon_b c_b^i)$ where $c_b^i$ corresponds to 1-AHAQ. DNA concentration while $c_f^i$ is the concentration of free 1-AHAQ in the experimental solution. ε and $\varepsilon_b$ are the molar extinction coefficients of 1-AHAQ and DNA.1-AHAQ, respectively.

Therefore, $(\Delta A/\Delta A_m)$ denotes the fraction of 1-AHAQ bound to DNA. Hence, one gets $(\Delta A/\Delta A_m)C_0 = [\mathrm{DNA.1\text{-}AHAQ}]$. Then Eq. (6) becomes

$$K_d = \frac{\left[C_0-\left(\frac{\Delta A}{\Delta A_m}\right)C_0\right]\left[C_D-\left(\frac{\Delta A}{\Delta A_m}\right)C_0\right]}{\left(\frac{\Delta A}{\Delta A_m}\right)C_0} \quad (7)$$

$$C_0\left(\frac{\Delta A}{\Delta A_m}\right)^2 - (C_0 + C_D + K_d)\left(\frac{\Delta A}{\Delta A_m}\right) + C_D = 0 \quad (8)$$

Experimental data from the binding studies were analyzed according to Eq. (8) by using the method of least square fit to determine $K_d$ and, hence, $K$. However, the evaluation of $K_d$ using this method requires the value of $\Delta A_m$ which was determined by a double reciprocal plot (Fig. 6a) of $1/\Delta A$ vs. $1/(C_D-C_0)$ according to Eq. (9) [12,14–16,74–78]. Using this method (Fig. 6a) the value of $K_d$ was also evaluated.

$$\frac{1}{\Delta A} = \frac{1}{\Delta A_m} + \frac{K_d}{\Delta A_m(C_D - C_0)} \quad (9)$$

Fig. 6b shows the binding isotherm of 1-AHAQ with DNA from which the apparent binding constant was determined by using Eq. (8) as $(1.20 \pm 0.08) \times 10^4\ \mathrm{M}^{-1}$. The double reciprocal plot (Fig. 6a) produced the apparent binding constant as $(1.56 \pm 0.10) \times 10^4\ \mathrm{M}^{-1}$. Using the plot of $A_0/(A-A_0)$ against the inverse of [DNA] (Fig. 5b), $K$ was obtained as $(1.09 \pm 0.11) \times 10^4\ \mathrm{M}^{-1}$ (summarized in Table 4). Comparing the values of K, it is clear that three methods for the determination of $K$ correlate excellently. The plot of $(\Delta A/\Delta A_m)$ vs. the mole ratio of 1-AHAQ to DNA bases [Fig. S5 (Supporting information)] produced two straight lines intersecting with each other at particular point which actually gives the bind site size or binding stoichiometry (n) in terms of DNA bases bound per molecule of 1-AHAQ [12,14–16,74–79]. In the present study '$n$' was established as $(6.52 \pm 0.42)$ bases, i.e., $(3.26 \pm 0.21)$ base pairs. It was then used to find the intrinsic binding constant K′, i.e. $(K \times n)$ which was observed as $(1.20 \times 10^4 \times 6.52)$, i.e., $(7.82 \pm 0.16) \times 10^4\ \mathrm{M}^{-1}$. In a very recent work [72] by using cyclic voltammetry and ethidiumbromide displacement assay we showed that 1-AHAQ intercalates DNA with an intrinsic binding constant in the order of $10^4\ \mathrm{M}^{-1}$ which justifies the method of present measurement.

Another important double reciprocal method used in an earlier study [80] was employed in the present study to find $K$ by using Eq. (10).

$$\frac{1}{f} = 1 + \frac{1}{K[\mathrm{DNA}]} \quad (10)$$

where f=fraction of total 1-AHAQ bound=$C_b/C_0$=[DNA.1-AHAQ]/$[1\text{-AHAQ}]_0$ = $\{(\Delta A/\Delta A_m)C_0\}/\ C_0=(\Delta A/\Delta A_m)$. [DNA] is concentration of DNA in bases in the experimental solution. It is

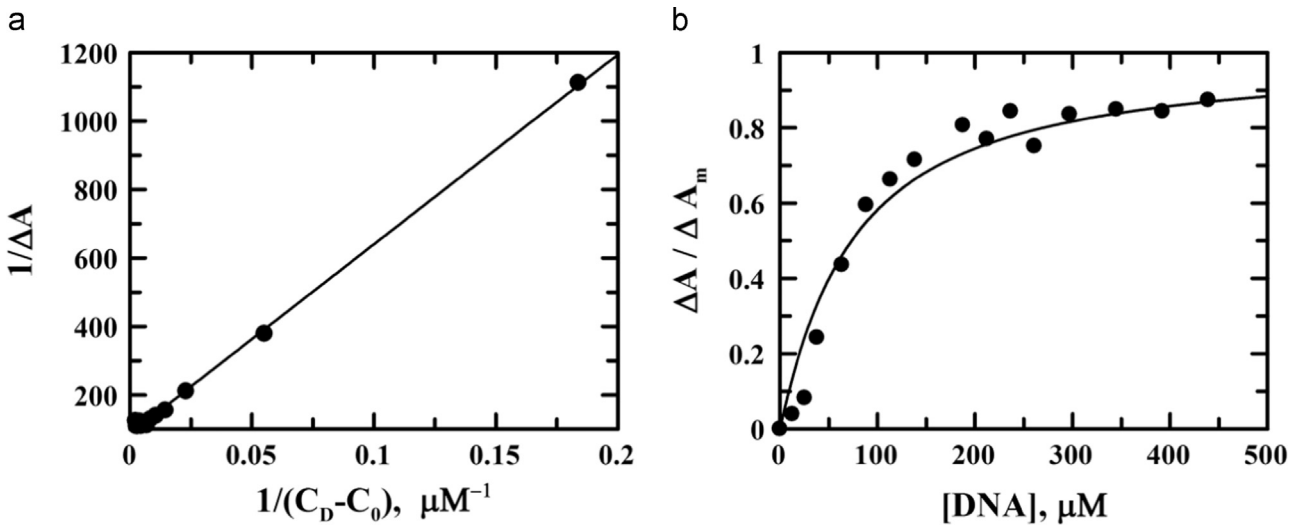


**Fig. 6.** (a) Double reciprocal plot of 1-AHAQ – calf thymus DNA interaction using UV–vis spectroscopy; $[1\text{-AHAQ}]_0$ = 20 μM, pH=7.4, [NaCl]=120 mM, 25 °C. (b). Binding isotherm of 1-AHAQ and calf thymus DNA and corresponding non-linear fit using UV–vis spectroscopy; $[1\text{-AHAQ}]_0$=20 μM, pH=7.4, [NaCl]=120 M, 25°C.

**Table 4**
Comparison of binding parameters obtained from different fitting models.

| Apparent binding constant ($K$) ($M^{-1}$) | | | | Binding site size ($n$) (Bases) | Intrinsic Binding Constant $K'$ $=(K\times n)$ ($M^{-1}$) |
|---|---|---|---|---|---|
| Double reciprocal plot using Eq. (2) | Non linear fit analysis using Eq. (8) | Double reciprocal plot using Eq. (9) | Double reciprocal plot using Eq. (10) | | |
| $(1.09\pm0.11)\times10^{4}$ | $(1.20\pm0.08)\times10^{4}$ | $(1.56\pm0.10)\times10^{4}$ | $(1.50\pm0.12)\times10^{4}$ | $(6.52\pm0.42)$ | $(7.82\pm0.16)\times0^{4}$ |

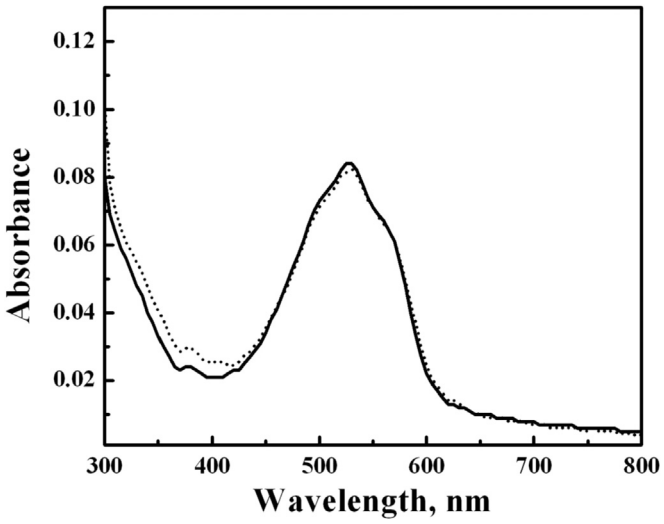


**Fig. 7.** Absorption spectra of 1-AHAQ in the absence (solid line) and presence (dotted line) of single stranded ct DNA in phosphate buffer at pH 7.4. [1-AHAQ] = 30 μM, [Phosphate Buffer]=50 μM, [NaCl]=120 mM, [ss DNA]=80 μM, 298.15 K.

important to mention here that this method is valid only for those experiments where the free DNA is present in large excess in comparison to that of the compound tested [79]. The present study followed this condition as we mentioned above, and that is the reason why such a double reciprocal plot [Fig. S5 (Supporting information)] should be useful in our case. Using the method, K was evaluated as $(1.50\pm0.12)\times10^{4}\ M^{-1}$ which corroborate nicely with the values observed from other methods (Table 4). A comparison of the present results with an earlier study [81] it can be said that intrinsic and apparent binding constants obtained in the present study are very close to that reported for mitoxantrone and other anthracycline drugs [81]. Oyaga*et al.* [59] showed that a strong binding of a molecule with DNA is a measure of cytotoxicity at cellular level which makes 1-AHAQ to be important in the area of anthracycline research. Further, the interaction of this category of compounds with DNA is also a significant step in their action as drug [4–8]. Thus, considering the binding affinity of the present molecule with DNA, one may expect that 1-AHAQ might be a potential antitumor agent like established anthracyclines.

### 3.8. Mode of interaction of 1-AHAQ with DNA

The nature of 1-AHAQ–DNA interaction was established by carrying out binding studies of 1-AHAQ with single-stranded ct DNA under the similar experimental conditions as mentioned above. An aliquot containing 1-AHAQ and single-stranded ct DNA (ss DNA) was prepared and UV–vis spectrum was measured. Fig. 7 shows the absorption spectra of 1-AHAQ and 1-AHAQ – ss DNA mixture which shows that the addition of ss DNA does not bring a significant change in the intensity of the peak at 530 nm. This clearly suggests that the chance of groove binding between DNA and 1-AHAQ is negligible. Thus, the hypochromic effect found in the interaction of 1-AHAQ with double-stranded ct DNA is definitely due to intercalation of the compound into DNA base pairs [Scheme SI (Supporting Information)].

A competitive binding study involving 1-AHAQ, double-stranded ct DNA and ethidium bromide (EB), an established DNA intercalator, was also done to establish the intercalation mode by monitoring fluorescence of the mixture in our very recent study [72]. The study confirmed that 1-AHAQ intercalates into the double-stranded DNA by replacing EB [72]. As mentioned above the intercalation of this class of molecules into DNA base pairs plays a key role in their drug action. Intercalation of 1-AHAQ into DNA base pairs and binding affinity of the current molecule with DNA being comparable to anthracycline drugs clearly suggest that the planar 9,10-anthraquinone unit of the molecule probably plays the role in its biological action. This may raise the hope that 1-AHAQ might be a potential antitumor agent like established anthracyclines. In order to see if these results lead to an induction of apoptosis in cancer cells, 1-AHAQ was applied to MDA-MB-231 breast adinocarcinoma cells and the outcomes of the entire studies were correlated.

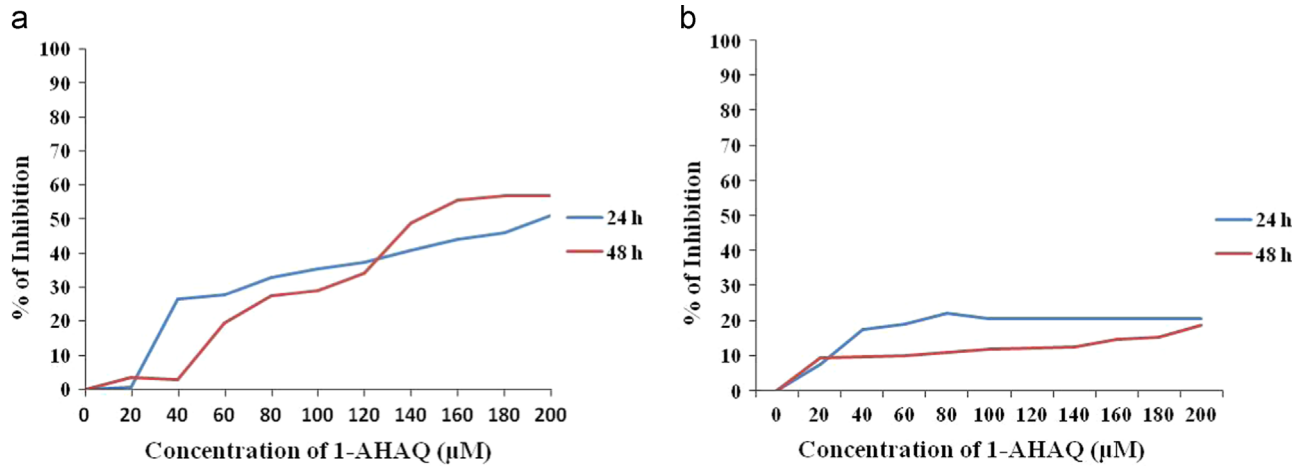


**Fig. 8.** (a) MTT assay for 1-AHAQ for 24 h and 48 h in MDAMB 231 cells. (b) MTT assay for 1-AHAQ for 24 h and 4 8 h in HBL-100 cells.

**Table 5**
Inhibitory concentration of 1-AHAQ against MDA-MB-231 breast adinocarcinoma and HBL-100 breast epithelial cells.

| Cell line | 1-AHAQ | | |
|---|---|---|---|
| | Inhibitory rates (%) | Concentration in (μM) | |
| | | 24 h | 48 h |
| MDA-MB-231 (breast adinocarcinoma cells) | 50 | 200 ± 0.02 | 140 ± 0.03 |
| HBL-100 (breast epithelial cells) | 20 | 200 ± 0.05 | 200 ± 0.02 |

### 3.9. Effect of 1-AHAQ on the viability of breast cancer cells

1-AHAQ was applied to MDA-MB-231 breast adinocarcinoma and HBL-100 breast epithelial cell lines and its inhibitory effect at different concentrations (20-200 μM) and time intervals (24 and 48 h) were investigated adopting MTT assay (Fig. 8). MTT is converted into purple-colored formazon product in cells with viable mitochondria whereas dead or dying cells lose this ability. Thus the color of the formazon and the subsequent solution in DMSO is indication of the metabolic viability or otherwise of the cells. It was observed that 1-AHAQ is cytotoxic to MDA-MB-231 breast adinocarcinoma cells in a manner dose-dependent and little if any on HBL-100 breast epithelial cells. Fig. 8 and Table 5 show the inhibitory rates and corresponding concentrations at which 1-AHAQ is cytotoxic to the adinocarcinomatous MDA-MB-231 cells. Results in Table- 5 clearly indicate that 1-AHAQ was able to cause 50% growth inhibition of the cancer cells at 200 μM concentration when incubated for 24 hours and at 140 μM concentration when incubated for 48 hours whereas it had almost no effect on normal cells with inhibition being only 20% at 200 μM when incubated for 24 hours as well as 48 hours. Thus 1-AHAQ behaves as a potential anticancer agent.

### 3.10. AO/EB staining

Apoptosis is a highly regulated physiological cell death. The cells undergoing this mechanism of death exhibit very specific morphologies. The affected cells shrink to small size, the nucleus also dereases in size accompanied by condensation of chromatin and fragmentation of DNA, blebbing of cell membrane, and apoptotic body formation. If treatment of MDA-MB-231 adinocarcinoma cells with 1-AHAQ results in these indicators of apoptosis was assessed adopting AO/EB staining. We adopted dual staining, AO and EB. AO was excited at 500 nm (DNA) and emits at 526 nm; EB is excited at 510 nm and emits at 595 nm. Since we used a Zeiss fluorescent microscope we used the nearest UV filter set 09 which excites between 450 and 490 nm and allows emission at 515 nm. In this staining method AO renders both live and dead cells to fluoresce, live in green and dead in shades of red. EB, on the other hand permeates only cells in which the membrane integrity has been lost, i.e., dead/unviable cells, and fluoresces in shades of red. Thus, EB permeates dead cells which fluoresce orange-red which are super-imposed to the red fluorescence of AO. Live cells allow only AO to permeate and fluoresce green. Cytological changes observed in the treated cells are classified into Four different nuclear features and fluorescence patterns are discernable on staining with AO and EB: (i) in viable cells nuclei are normal, so fluoresce green; (ii) cells in an early phase of apoptosis in which the nuclei are condensed fluoresce orange-green; (iii) cells in a late phase of apoptosis , the chromatin is highly condensed or fragmented and fluoresce orange to red; and iv) cells undergoing necrotic death do not show fragmentation of chromatin and fluoresce orange to red. In 1-AHAQ-treated cancer cells all these morphological changes could be observed. The data in respect of treatment with $IC_{50}$ concentration of 1-AHAQ for 24 h are presented in Fig. 9a, which reveal that apoptotic morphology was in preponderance but there were a few cells with necrotic morphologies also. The data presented in Fig. 9b reveal that 1-AHAQ is efficient in inducing apoptotic death in MDA-MB-231 breast adinocarcinoma cell rather selectively.

### 3.11. Hoechst staining

Hoechst 33528 staining specifically reveals morphological changes in the nucleus and chromatin. The nuclei of untreated and control cells were spherical and fluoresced uniformly, and the chromatin was intact. The cells treated with 24 h $IC_{50}$ concentration of 1-AHAQ showed changes in the morphology of their nuclei such as chromatin marginalization, condensation and fragmentation. Fig. 10 indicates the apoptotic nuclear morphologies as brought up by 1-AHAQ-

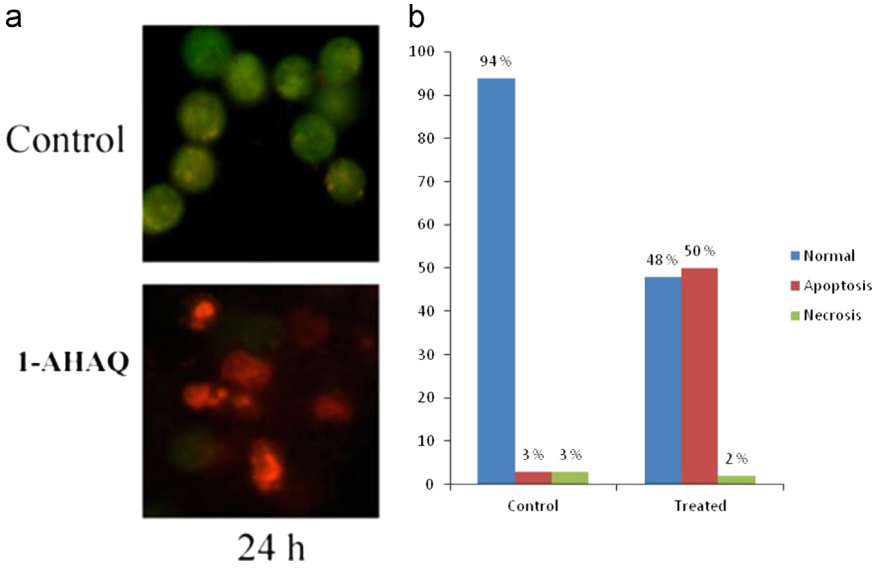


**Fig. 9.** The effect of 1-AHAQ on MDAMB 231 cells with Acridine orange and ethidium bromide staining. (a) Representative morphological changes observed against MDAMB 231 cells after 24 h incubation with 1-AHAQ. (b) Relative percentage of morphological changes was determined and classified into three categories: viable, apoptosis and necrosis as compared with the control cells after 24 h incubation.

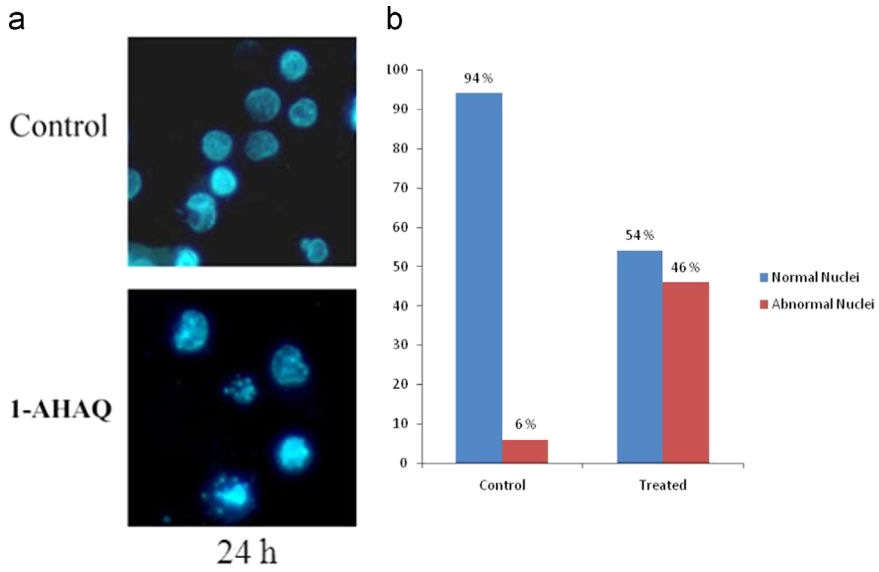


**Fig. 10.** The effect of 1-AHAQ on MDAMB 231 cells with Hoechst staining. (a) Representative morphological changes observed against MDAMB 231 cells after 24 h incubation with 1-AHAQ. (b) Relative percentage of morphological changes was determined and classified into two categories: Normal and abnormal nuclei as compared with the control cells after 24h incubation.

treatment. At the concentration of 1-AHAQ that kills 50% of cells, 46% had abnormal nuclei. Considering the overall perspective of the apoptotic effect of 1-AHAQ on MDA-MB-231 breast adinocarcinoma cells and its mode of action therein one may suggest that the less expensive 1-AHAQ may be used as an affordable alternative to the very expensive anthracycline drugs in the near future.

## 4. Conclusions

The single crystal structure of 1-AHAQ, an analogue of anthracycline drugs, was evaluated in the present study. The outcome is a valuable addition in the area of structure and bonding of anthracyclines as there are not many reports in this area. The geometry of the molecule was optimized by computational methods that correlate well with the single crystal structure. Geometrical parameters obtained from both the computational and experimental results were found to be in a rational agreement. Two types of hydrogen bonds were observed in the molecule as established by X-ray diffraction study, DFT and NBO analysis. The theoretical vibrational spectra of the molecule studied by VEDA by using PED analysis, corroborates with the experimental values excellently. Theoretical studies on vibrational and molecular spectra determined the mode of vibration and transitions involved. The electrochemical study showed that 1-AHAQ undergoes quasi-reversible single step reduction involving two electrons in aqueous solution at physiological pH (7.4) like anthracycline anticancer drugs. The molecule has a significant affinity for binding DNA and it intercalates into DNA base pairs through its planar 9,10-anthraquinone unit. It induces apoptosis in MDA-MB-231 breast adinocarcinoma cells while its cytotxicity to the HBL-100 normal breast epithelial cell is ignorable. The electrochemical aspects, structural characteristics and the affinity of the molecule to interact with DNA possibly play role in its action as a potential antitumor agent.

## Conflict of interest

The authors declare no conflict of interests.

## Acknowledgment

PSG is very much thankful to UGC, New Delhi, India, for the financial support through the Major Research Project (File no. 41-225/2012 (SR) dated 18th July 2012). MAA acknowledges the grant from Doerenkamp-Zbinden Foundation, Switzerland, for establishment of the Mahatma Gandhi-Doerenkamp Center.

## Appendix A. Supplementary material

Supplementary data associated with this article can be found in the online version at http://dx.doi.org/10.1016/j.bbrep.2015.10.008.

## References

[1] J.G. Hardman, A.G. Gilman, L.E. Limbird, Goodman and Gilman's the Pharmacological Basis of Therapeutics, 9th ed, McGraw-Hill Companies, New York, 1996.
[2] F.Q. Hu, L.N. Liu, Y.Z. Du, H. Yuan, Biomaterials 30 (2009) 6955–6963.
[3] K.H. Lim, H.S. Kim, Y.M. Yang, S.D. Lee, W.B. Kim, J. Yang, J.G. Park, Cancer Chemother. Pharmacol. 40 (1997) 23–30.
[4] G.E. Kellogg, J.N. Scarsdale, F.A. Fornari, Nucleic Acids Res. 26 (1998) 4721–4732.
[5] M. Binaschi, G. Capranico, Bo. L. Dal, F. Zunino, Mol. Pharmacol. 62 (1997) 1053–1057.
[6] D.A. Gewirtz, Biochem. Pharmacol. 57 (1999) 727–741.
[7] S. Moro, G.L. Beretta, D. Dal Ben, J. Nitiss, M. Palumbo, G. Capranico, Biochemistry 3 (2004) 7503–7513.
[8] D. Dal Ben, M. Palumbo, G. Zagotto, G. Capranico, S. Moro, Curr. Pharm. Des. 13 (2007) 2766–2780.
[9] L. Zhu, X. Cao, W. Chen, G. Zhang, D. Sun, P.G. Wang, Bioorg. Med. Chem. 13 (2005) 6381–6387.
[10] W. Priebe, Molecules 5 (2000) 299–301.
[11] Y.S. Rho, R. Park, S.Y. Kim, D.J. Yoo, Bull. Korean Chem. Soc. 31 (2010) 69–74.
[12] P.S. Guin, S. Das, P.C. Mandal, J. Inorg. Biochem. 103 (2009) 1702–1710.
[13] P.S. Guin, P.C. Mandal, S. Das, Rad. Phys. Chem. 89 (2013) 38–42.
[14] P.S. Guin, S. Das, P.C. Mandal, J. Phys. Org. Chem. 23 (2010) 477–482.
[15] P.S. Guin, S. Das, P.C. Mandal, J. Sol. Chem. 40 (2011) 492–501.
[16] P. Das, P.S. Guin, P.C. Mandal, M. Paul, S. Paul, S. Das, J. Phys. Org. Chem. 24 (2011) 774–785.
[17] S. Rossi, C. Tabolacci, A. Lentini, B. Provenzano, F. Carlomosti, S. Frezzotti, S. Beninati, Anticancer Res. 30 (2010) 445–449.
[18] J. Blasiak, E. Gloc, M. Warszawski, Acta Biochim. Pol. 49 (2002) 145–155.
[19] J. Kapuscinski, Z. Daizynkiewicz, Proc. Nat. Acad. Sci. U.S.A. 83 (1986) 6302–6306.
[20] A.L. Ellis, J.K. Randolph, B.R. Conway, D.A. Gewirtz, Biochem. Pharmacol. 39

(2012) 1549–1556.
[21] B.H. Trachtenberg, D.C. Landy, V.I. Franco, J.M. Henkel, E.J. Pearson, T.L. Miller, S.E. Lipshultz, Pediatr. Cardiol. 32 (2011) 342–353.
[22] Y. Shi, M. Moon, S. Dawood, B. McManus, P.P. Liu, Herz 36 (2011) 296–305.
[23] D. Outomuro, D.R. Grana, F. Azzato, J. Milei, Int. J. Cardiol. 117 (2007) 6–15.
[24] V.J. Ferrans, Cancer Treat. Rep. 62 (1978) 955–961.
[25] D. Barasch, O. Zipori, I. Ringel, I. Ginsburg, A. Samuni, J. Katzhendler, Eur. J. Med. 34 (1999) 597–615.
[26] G.E. Kellogg, J.N. Scarsdale, F.A. Fornari, Nucleic Acids Res. 26 (1998) 4721–4732.
[27] H.M. Zhang, N.Q.J. Li, Pharm. Biomed. Anal. 22 (2000) 67–73.
[28] J.B. Chaires, Molecular recognition of DNA, in: L.H. Hurley, J.B. Chaires (Eds.), Advances in DNA Sequence-Specific Agents, vol. 2, JAI Press, Greenwich, CT, 1996.
[29] A.H.–J. Wang, Structure–activity studies of anthracycline—DNA complexe, in: S. Neidle, M. Waring (Eds.), Molecular Aspects of Anticancer Drug–DNA Interactions, vol. 1, CRC Press, FL, Boca Raton, 1993.
[30] F. Arcamone, G. Cassinelli, F.D. Matteo, S. Forenza, M.C. Ripamonti, G. Rivola, A. Vigevani, J. Clardy, T. McCabe, J. Am. Chem. Soc. 102 (1980) 1462–1463.
[31] S.K.J. Arora, Biomol. Struct. Dyn. 3 (1985) 377–385.
[32] S. Roy, P.S. Guin, J. Electrochem. Soc. 162 (2015) H124–H131.
[33] S. Roy, P. Mondal, P.S. Sengupta, D. Dhak, R.C. Santra, S. Das, P.S. Guin, Dalton Trans. 44 (2015) 5428–5440.
[34] O. Warburg, W. Christian, Biochem. Z. 310 (1942) 384–421.
[35] M.M.S. Silva, I.T. Cavalcanti, M.F. Barroso, M.G.F. Sales, R.F. Dutra, J. Chem. Sci. 122 (2010) 911–917.
[36] Bruker AXS, SMART and SAINT, Bruker AXS Inc., Madison, WI, USA, 1998.
[37] G.M.Sheldrick, SHELXS-97, Programs for X-ray Crystals Structure Solution, University of Gottingen, Germany, 1997.
[38] A. Mallik, T. Mandal, R. Pal, D. Ghosal, A. Patra, Synlett 23 (2012) 2459–2462.
[39] A.L. Spek., J. Appl. Crystallogr. 36 (2003) 7–13.
[40] L.J. Farrugia, J. Appl. Crystallogr. 30 (1997) 565–566.
[41] L.J. Farrugia., J. Appl. Crystallogr. 32 (1999) 837–838.
[42] C. Lee, W. Yang, R.G. Parr, Phy. Rev. B 37 (1998) 785–789.
[43] R.H. Hertwig, W. Koch, Chem. Phys. Let. 268 (1997) 345–351.
[44] J.P. Perdew, K. Burke, M. Ernzerhof, Phys. Rev. Lett. 7 (1996) 3865–3868.
[45] V. Barone, M. Cossi, J. Phys. Chem. A 102 (1998) 1995–2001.
[46] M. Cossi, N. Rega, G. Scalmani, V. Barone, J. Comput. Chem. 24 (2003) 669–681.
[47] A. Klamt, G. Schüürmann, J. Chem. Soc. Perkin Trans. 2 (1993) 799–805.
[48] J. Andzelm, C. Kölmel, A. Klamt, J. Chem. Phys. 103 (1995) 9312–9320.
[49] M.H. Jamroz, Vibrational Energy Distribution Analysis VEDA, vol. 4, 2004.
[50] J.B. Foresman, A. Frish, Exploring Chemistry with Electronic Structure Methods, Gaussian, Inc., Pittsburgh, PA, USA (2000), p. 64.
[51] A.E. Reed, L.A. Curtiss, F. Weinhold, Chem. Rev. 88 (1988) 899–926.
[52] A. Ebrahimia, F. Deyhimi, H. Roohi, J. Mol. Struct. (THEOCHEM) 626 (2003) 223–229.
[53] S. Banerjee, P.S. Sengupta, A.K. Mukherjee, J. Mol. Struct. THEOCHEM 913 (2009) 97–106.
[54] M.J. Frisch, G.W. Trucks, H.B. Schlegel, G.E. Scuseria, M.A. Robb, J.R. Cheeseman, G. Scalmani, V. Barone, B. Mennucci, G.A. Petersson, H. Nakatsuji, M. Caricato, X. Li, H.P. Hratchian, A.F. Izmaylov, J. Bloino, G. Zheng, J.L. Sonnenberg, M. Hada, M. Ehara, K. Toyota, R. Fukuda, J. Hasegawa, M. Ishida, T. Nakajima, Y. Honda, O. Kitao, H. Nakai, T. Vreven, J.A. Montgomery, J.E. Peralta, F. Ogliaro, M. Bearpark, J.J. Heyd, E. Brothers, K.N. Kudin, V.N. Staroverov, R. Kobayashi, J. Normand, K. Raghavachari, A. Rendell, J.C. Burant, S.S. Iyengar, J. Tomasi, M. Cossi, N. Rega, J.M. Millam, M. Klene, J.E. Knox, J.B. Cross, V. Bakken, C. Adamo, J. Jaramillo, R. Gomperts, R.E. Stratmann, O. Yazyev, A.J. Austin, R. Cammi, C. Pomelli, J.W. Ochterski, R.L. Martin, K. Morokuma, V. G. Zakrzewski, G.A. Voth, P. Salvador, J.J. Dannenberg, S. Dapprich, A.D. Daniels, Ö. Farkas, J.B. Foresman, J.V. Ortiz, J. Cioslowski, D.J. Fox, Gaussian 09, Revision C.01, Gaussian, Inc., Wallingford CT, 2009.
[55] T. Mosmann, J. Immunol. Methods 65 (1983) 55–63.
[56] D.L. Spector, R.D. Goldman, L.A. Leinwand, Cell: A Laboratory Manual, Culture and Biochemical Analysis of Cells, Cold Spring Harbor Laboratory Press, Cold Spring Harbor, New York (1998), p. 341–349.
[57] S.A. Latt, G. Stetten, L.A. Juergens, H.F. Willard, C.D. Scher, J. Histochem. Cytochem. 23 (1975) 493–505.
[58] Y. Zhu, F. Ma, K. Ma, L. Cao, L. Zhao, J. Chem. Sci. 123 (2011) 687–696.
[59] S.C. Oyaga, J.C. Valdés, S.B. Paez, K.H. Marquez, J. Theor. Chem. (2013) (Article ID 526569, 8 pp.).
[60] A.V. Iogansen, Spectrochim. Acta. Part A 55 (1999) 1585–1612.
[61] V.Y. Fain, B.E. Zaitsev, M.A. Ryabov, Rus. J. Coord. Chem. 36 (2010) 396–400.
[62] Y. Zhao, D.G. Truhlar, Acc. Chem. Res. 41 (2008) 157–167.
[63] Y. Zhao, D.G. Truhlar, Theor. Chem. Acc. 120 (2008) 215–241.
[64] K.W. Wiberg, Tetrahedron 24 (1968) 1083–1096.
[65] K. Kano, T. Konse, N. Nishimura, T. Kubota, Bull. Chem. Soc. Jpn. 57 (1984) 2383–2390.
[66] Y. Hahn, H.Y. Lee, Arch. Pharm. Res. 27 (2004) 31–34.
[67] P.S. Guin, S. Das, Int. J. Electrochem. (2014) (Article ID 517371, 8 pp.).
[68] V. Kertesz, J.Q. Chambers, N.A. Mullenix, Electrochim. Acta 45 (1999) 1095–1104.
[69] R. Fakuda, S. Takenaka, M. Takagi, J. Chem. Soc. Chem. Commun. (1990) 1028–1030.
[70] E.C. Long, J.K. Barton, Acc. Chem. Res. 23 (1990) 271–273.
[71] C. Cantor, P.R. Schimmel, Biophysical Chemistry (3 volumes) Part I: The Conformation of Biological Macromolecules. Part II: Techniques for the Study of Biological Structure and Function. Part III: The Behavior of Biological Macromolecules, Freeman WH, San Fransisco, 1980.
[72] S. Roy, P.S. Guin, J. Mol. Liq. 211 (2015) 846–853.
[73] I. Takenaka, T. Ihara, M. Takagi, J. Chem. Soc. Chem. Commun. (1990) 1485–1487.
[74] X.J. Dang, M.Y. Nie, J. Tong, H.L. Li, J. Electroanal. Chem. 448 (1998) 61–67.
[75] T. Deb, D. Chakraborty, P.S. Guin, M.B. Saha, G. Chakrabarti, S. Das, Chem. Biol. Interact. 18 (2011) 206–214.
[76] S. Roy, R. Banerjee, M. Sarkar, J. Inorg. Biochem. 100 (2006) 1320–1331.
[77] S. Chakrabarti, B. Bhattacharyya, D. Dasgupta, J. Phys. Chem. B 106 (2008) 6947–6953.
[78] M.A. Mir, S. Majee, S. Das, D. Dasgupta, Bioorg. Med. Chem. 11 (2003) 2791–2801.
[79] P.S. Guin, P.C. Mandal, S. Das, ChemPlusChem 77 (2012) 361–369.
[80] F. Frezard, A. Garnier-Suillerot, Biochim. Biophys. Acta 1036 (1990) 121–127.
[81] N. Li, Y. Ma, C. Yang, L. Guo, X. Yang, Biophys. Chem. 116 (2005) 199–205.